UAH Research Report No. 194

LOW-GRAVITY PROCESSING OF SUPERCONDUCTING COMPOUNDS

by

Guenther H. Otto

FINAL REPORT

Contract NAS8-31768

Prepared for

National Aeronautics and Space Administration
George C. Marshall Space Flight Center
Marshall Space Flight Center, Alabama 35812

Submitted by

The University of Alabama in Huntsville
School of Science and Engineering
Huntsville, Alabama 35807

November 1976

UAH Research Report No. 194

LOW-GRAVITY PROCESSING OF SUPERCONDUCTING COMPOUNDS

by

Guenther H. Otto

FINAL REPORT

Contract NAS8-31768

Prepared for

National Aeronautics and Space Administration
George C. Marshall Space Flight Center
Marshall Space Flight Center, Alabama 35812

Submitted by

The University of Alabama in Huntsville
School of Science and Engineering
Huntsville, Alabama 35807

November 1976

PREFACE

This Final Report contains the results of work performed during the period of 15 December 1975 to 31 October 1976 under Contract NAS8-31768. The achievements are derived from a cooperative research effort between NASA's Marshall Space Flight Center and The University of Alabama in Huntsville using the facilities of the Space Sciences Laboratory. Dr. Lewis L. Lacy served as the technical monitor of this contract.

TABLE OF CONTENTS

LIST OF FIGURES

LIST OF TABLES

ABSTRACT

Low gravity conditions can be sustained on earth for several seconds in an evacuated drop tube. Since radiation cooling is most effective at high temperatures, the refractive metals and alloys are prime candidates for free fall solidification. In this report, the results of initial experiments on droplet formation, droplet release, critical size and evaporation losses are given. The time required for free fall solidification of different size droplets is calculated and will serve as a base-line for the future installation of the free fall tube. The materials studied were copper, niobium and vanadium and a niobium-tin alloys. Improvements in purity, composition, homogeneity and stoichiometry are expected during free fall solidification of niobium based alloys which should become evident in an increase in the superconducting transition temperature.

I. Introduction

Recent experiments on Skylab [1] and the Apollo-Soyuz Test Project [2] have shown the influence of low gravity conditions on the solidification of various alloys. These experiments made use of the long-term low-gravity environment associated with spacecrafts in earth orbit. In preparation of similar experiments for Spacelab it seems important to construct a facility which allows generation of short-duration low-gravity conditions in a laboratory scale to test certain materials and alloys for their suitability of space processing.

On earth, short-duration low-gravity conditions can be sustained for the duration of several seconds in airplanes, drop towers or drop tubes [3]. Of these facilities the most convenient and economic is a drop tube. Low gravity conditions can be sustained in an evacuated tube of 30 meters length for 2.5 seconds. This time span is sufficient to solidify small droplets of liquid metals or alloys having a high melting temperature. Prime candidates for a drop tube would be materials with melting temperatures above 1500 ^{o}C, especially alloys of the refractory metals or glasses.

To evaluate the feasibility of a drop tube, preliminary studies have been performed on the production of various size droplets and their detachment from supporting niobium and copper rods. These studies do not require the free-fall tube and serve as a test for the melting apparatus and the vacuum system.† But the necessary data can be collected to calculate the free-fall solidification times for selected elements and alloys. By controlling the droplet size, the solidification time required can be matched with the available free-fall distance.

At these high temperatures, evaporation losses became important and it was possible to calculate the expected evaporation rates from first principles. Since the refractive elements are the main constituents in superconducting A-15 compounds, data for the pure elements niobium and vanadium will be presented.

---

† A drop tube with a length of 30 meters is presently (being) installed at the Marshall Space Flight Center.

Prime candidates for future drop tube experiments are compounds with A-15 structure. The reaction temperature and reaction mechanism for the peritectic reaction of the compounds will be given. Since the transition temperature of these compounds is initially controlled by composition, stoichiometry and homogeneity, improvements in those parameters by free-fall solidification should lead to an increase in the transition temperature of the compound [4] The necessary data for evaporation rates and melting temperatures for the constituents have been collected to better understand the criteria for the free-fall solidification of the particular compounds.

The drop tube also allows practicing the principle of containerless processing which reduces contamination of the sample. Although the time span of some seconds will not be sufficient to obtain optimum samples, the trends of selected parameters can be used to determine the Salient improvements resulting from low-gravity processing. By specifying selected parameters, a drop tube experiment can lead to a more meaningful longer term experiment as for example on a rocket or Spacelab flight.

II. Aspects of Free-Fall Solidification

A. Radiation Cooling

A heated material transmits energy to the cooler surroundings in the form of radiation, convection and conduction. If we consider a liquid metal droplet falling in an evacuated tube, energy will be lost by blackbody radiation only. According to the Stephan-Boltzmann relation, the amount of radiation is proportional to the fourth power of the absolute temperature and is expressed by

$$\dot{Q} = \sigma \, E \, A \, (T_2^4 - T_1^4). \qquad (1)$$

In this expression, T_2 is the temperature of the liquid metal, T_1 is the temperature of the surroundings, A is the surface area of the droplet, E is the total emissivity of the liquid metal and σ is the Boltzmann constant with a value of $\sigma = 5.67 \times 10^{-12}$ Watt cm^{-2} deg^{-4}. Since we will limit ourselves to the free-fall solidification of metallic droplets, T_2 will be the isothermal melting temperature of the alloy. Assuming two materials with the same emissivities and surface area, the radiated

energy at 2000 ^{o}C is 2.7 times larger when compared with 1500 ^{o}C. At 1000 ^{o}C the ratio of the radiated energies is $\dot{Q}(2000\ ^{o}C)/\dot{Q}(1000\ ^{o}C) = 10.2$. Accordingly, the rate of solidification 2000 ^{o}C will be faster by the same amount for materials with the same heat of fusion.

The ratio by which the surface radiation deviates from that of an ideal black-body is denoted as the surface's emissivity. For most real materials, the emissivity varies as a function of wave length as well as temperature. Normally, clean metallic surfaces having a high reflevtivity also have a low value of radiant emittance. The emissivity increases when oxide layers are formed. As can be seen from handbook tables [5], the emissivities at 2000 ^{o}C for refractive metals are situated between 0.24 and 0.28. The data for some candidate materials at different temperatures are listed in Table 1.

As could be seen, the energy balance of a liquid droplet in vacuum is determined by the Stephan-Boltzmann relation. The time required for solidification of a specific material during free-fall can be derived from eq. (1) by integration.

B. Solidification Times for Selected Elements

Superconducting compounds with the A-15 structure are mainly composed of the refractive elements niobium, vanadium, and tantalum with the balance consisting of non-transition elements. It is, therefore opportune to first consider the properties of the high melting constituents before dealing with the compound materials.

As can be seen from Table 1, the melting temperatures for Nb, Ta, V are very high and the radiative loss rates are distributed accordingly. The time required for free-fall solidification will be given by the time required to radiate off the latent heat of fusion. Integrating eq. (1) and using the data of Table 1 with an average emissivity of E = .25, the following relation is obtained for <u>niobium</u>:

$$t = MC/E\sigma A(T_2^4 - T_1^4) \text{ or } t\ (\text{sec.}) = 0.0521\ MC/A \qquad (2)$$

where M is the mass of the droplet in gram, C the heat of fusion in cal/g and A the surface area of the droplet in cm^2. As can be seen, the solidification time is proportional to the mass and inversely proportional to the surface area of the droplet. But since the mass and area are

TABLE 1

DATA FOR A-15 CONSTITUENTS [5.6]

	Nb	V	Ta
Density (g/cm^3)	8.4	6.1	16.6
Cp (cal/g K) at 25 ^{o}C	0.064	0.0334	0.116
Melting Point (^{o}C)	2470	1890	2996
Boiling Point (^{o}C)	4740	3380	5425
Heat of Fusion (cal/g)	68	98	41
Lin Expans. ($x10^{-6}$ $^{o}C^{-1}$)	7	8.	6.5
Therm Cond. (W/cm ^{o}C) RT	0.52	0.60	0.54
Spec. Heat of Liquid Metal at 2000 ^{o}C (cal/g ^{o}C)	0.175	0.207	0.040
Vapor Press. of 10^{-9} atm (^{o}C)	2232	1591	2495
10^{-6} atm (^{o}C)	2721	1948	3025
Emissivity, E 1500 ^{o}C	0.19	--	0.21
2000 ^{o}C	0.24	--	0.26
Black-body Radiation at Melting Point (W/cm^2)	322	124.2	648

correlated by the density, the solidification time will be proportional to the diameter of the droplet.

The calculated solidification times for droplets of niobium and vanadium are given in Fig. 1. For vanadium, the numerical constant of 0.135 has been used in eq. (2). The upper boundary of the hatched region in Fig. 1 gives the time required for isothermal solidification of a spherical sample, whereas, the lower boundary illustrates the time required for an additional cooling from 100 ^{o}C above the melting temperature to 100 ^{o}C below melting temperature. Due to the higher radiative losses of solidifying niobium in comparison with vanadium, a Nb particle solidifies considerably faster than a vanadium droplet of the same mass. Doubling of the available free-fall duration would allow an eightfold increase of the mass of the solidifying droplet. A free-fall time of 2.5 sec. allows the solidification of a 600 mg niobium sample or a vanadium sample of 30 mg.

Figure 2 shows the same data as Figure 1, but we have plotted here the mass of a solidifying droplet against the free-fall distance required for solidification. This figure also includes the time required for cooling from 100 ^{o}C above to 100 ^{o}C below the melting temperature. These figures can be used to find for a given free-fall distance the maximum size and mass of vanadium and niobium droplets which still can be solidified. The hatched region indicates how much low-gravity time must be sacrificed for an additional cooling from 100 ^{o}C above to 100 ^{o}C below the melting temperature.

C. Characteristic Data for A-15 Compounds

Intermetallic compounds with the A-15 structure are formed by the transition elements V, Nb, Ta, Cr, Mo, and W with non-transition or transition elements. The general chemical description for the compounds is A_3B, where A represents a transition element. There are about 70 compounds known, which exhibit the A-15 structure [7]. Eight of the binary compounds have transition temperatures above 10K, and these materials are listed with their transition temperatures and melting

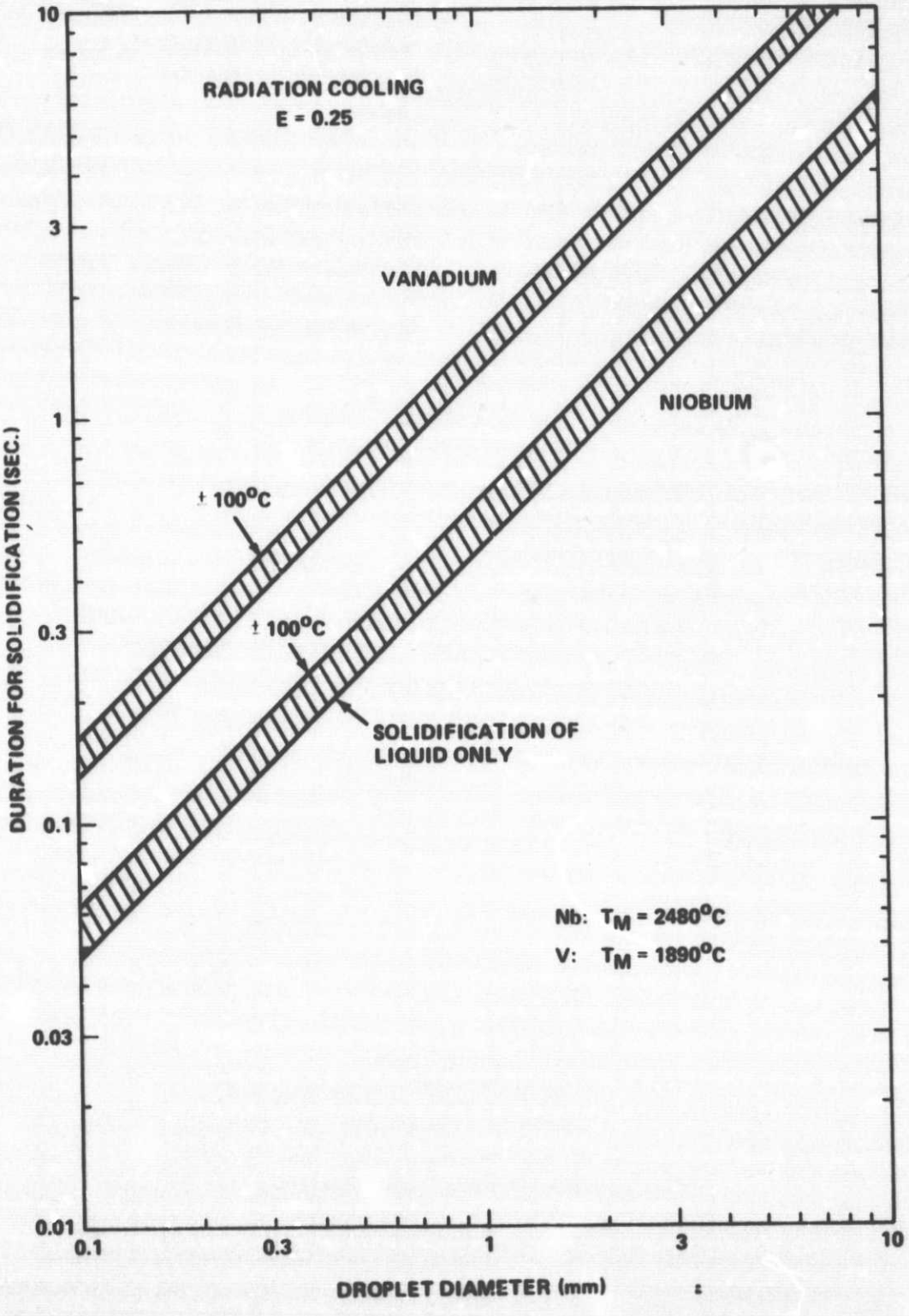

Figure 1. The required time for solidification of different size niobium and vanadium droplets. The upper boundary takes into account the additional time required for cooling from 100 °C above the melting temperature to 100 °C below.

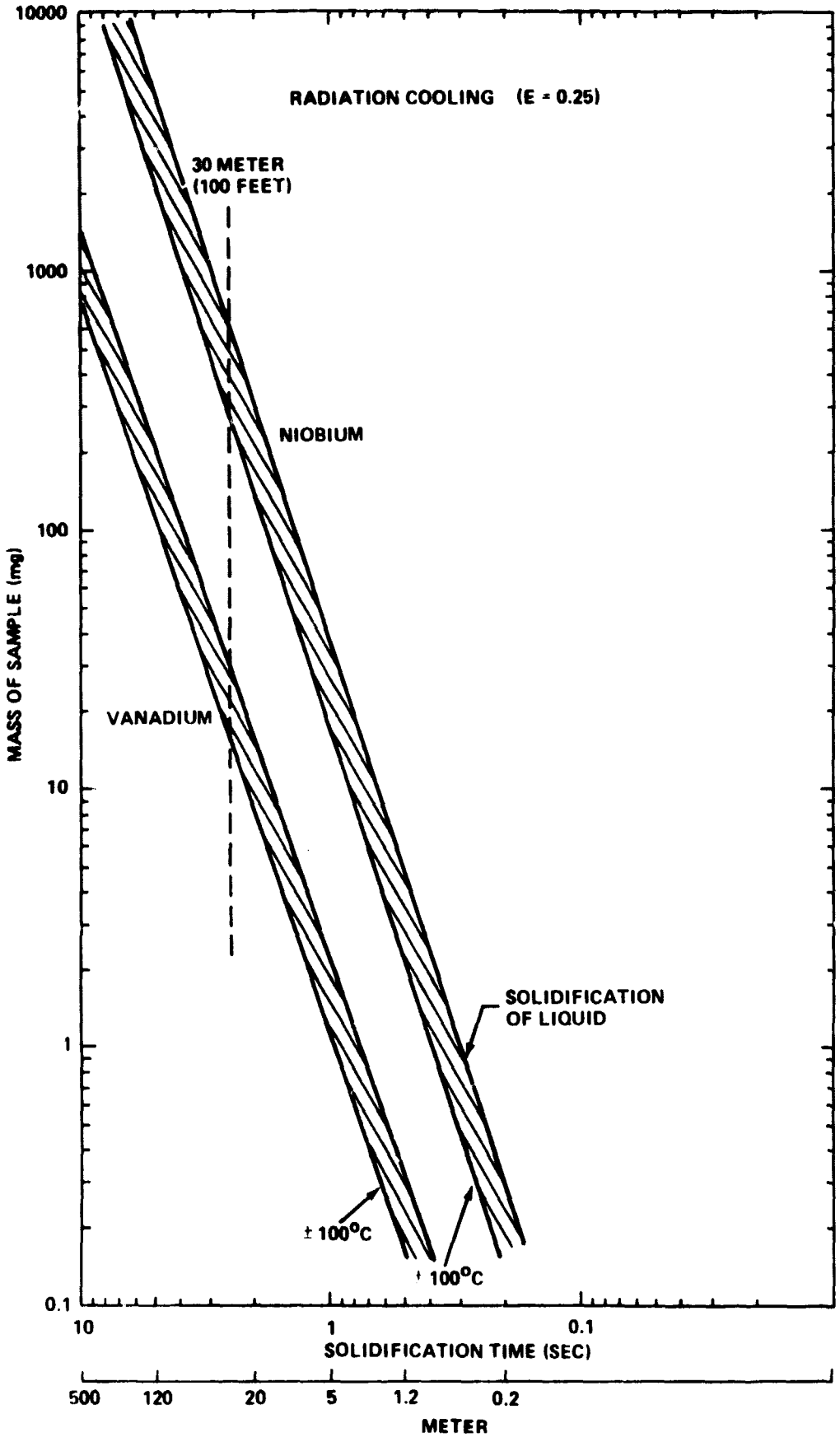

Figure 2. The solidification time for different mass Nb and V droplets. The upper boundary of the hatched region is calculated for isothermal solidification. The lower boundary takes into account the additional time required for cooling from 100 °C above to 100 °C below the melting temperature.

temperatures in Table 2. The basic construction plan of a unit cell is cubic. The B atoms form a bcc sublattice, while the A atoms are situated pair-wise on the 6 faces of the bcc unit cell as shown in Fig. 3. Each unit cell contains 8 atoms. In a stoichiometric and well-ordered compound, the A atoms form three-dimensional linear chains in which the A atoms are about ten percent closer to each other than in the pure element. It is postulated that the unique superconducting properties of the A-15 compounds are mainly based on the linear chains possible with this structure and on the degree of interatomic order achieved [8].

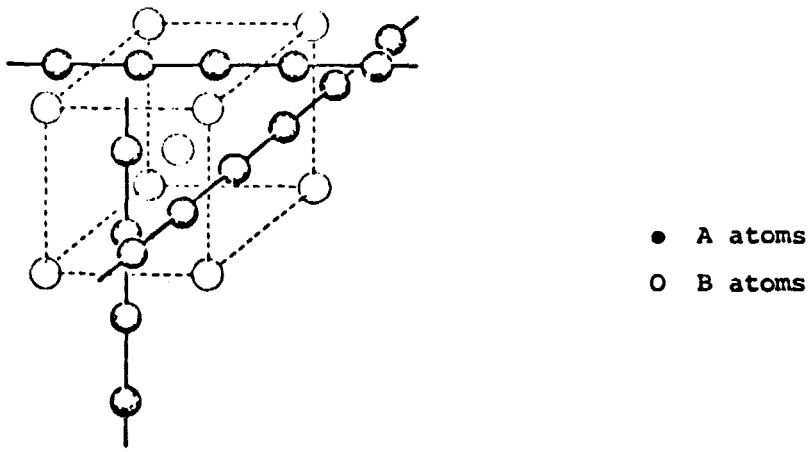

Figure 3: Atomic arrangement for A_3B compounds of the A-15 type structure. Solid circles represent A atom sites. Open circles represent B atom sites. For clarity, atoms on three of the six cube faces have been omitted. Note that the extension of the A chains is emphasized.

D. Mechanism of Peritectic Reaction

Most of the A-15 compounds form by peritectic reaction from the melt [25, 26, 27]. The temperature for this reaction ranges from 1300 ^{o}C for V_3Ga to approximately 2200 ^{o}C for Nb_3Al. A representative section of the Nb-Sn phase diagram is given in Fig. 4. It is characteristic in

TABLE 2

High T_c A-15 Superconductors

Compound	Status	T_c (K)	Melting Temp. (^oC)	References
Nb_3Ge	thin film	23.2		15
Nb_3Ge	quenched	17		16
Nb_3Ge	as-cast	6.9	~1910	17, 9
$Nb_3(Al, Ge)$*	annealed	20.7		18
$Nb_3(Al, Ge)$*	as-cast	18.8	--	17
Nb_3Al	annealed	18.72		19
Nb_3Al	as-cast	17.75	2200	19, 10
Nb_3Sn	annealed	18.05		20
Nb_3Sn	as-cast	17.8	1980	17, 11
V_3Si	annealed	17.05		18
V_3Si	as-cast	16.95	1970	20, 12
V_3Ga	annealed	14.5		20
V_3Ga	as-cast	13.65	1300†	21, 13
Nb_3Ga	annealed	16.1		17
Nb_3Ga	as-cast	15.6	1850	17, 14
Nb_3Ga	quenched	20.7		22
Nb_3Au	annealed	11.3		23
Nb_3Au	as-cast	9.9	1560†	23, 24
Nb_3Pt	annealed	10.7		23
Nb_3Pt	as-cast	8.6	~2000	23, 26

*Nominal composition: $Nb_3(Al_{0.75}Ge_{0.25})$

†Solid State reaction

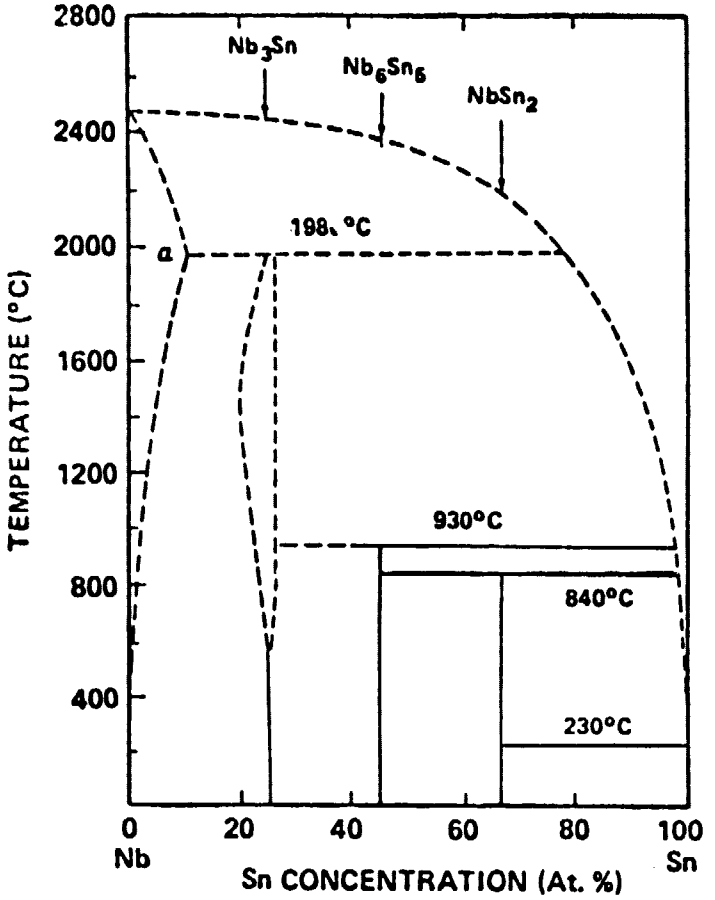

Figure 4: The Nb-Sn phase diagram showing the peritectic formation of Nb_3Sn [11].

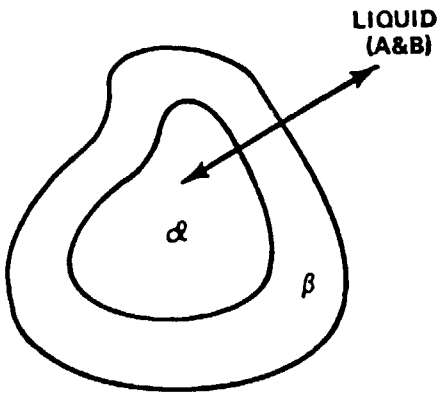

Figure 5: Schematic of the liquid and solid phase interation in a peritectic reaction.

a peritectic reaction that a solid and a liquid phase are involved to form the compound. In this process, the melt reacts with the precipitated primary solid solution (αNb) to form the A-15 compound (β-phase) according to the following schematic:

$$\alpha + \text{liquid} \rightleftharpoons \beta$$

The α-phase herein denotes the primary solid solution, like α-Nb. The peritectic reaction starts on the interface of α and the liquid. As a result, the α-crystallite is surrounded by a layer of the β-phase (compound) as schematically shown in Fig. 5. The peritectic reaction can only progress at the rate in which the B component (Sn) is delivered through β into the α-phase or at the rate in which A (Nb) can diffuse through the compound. This fact implies that the reaction rate is determined by the diffusivity of the A or B component in the solid β-phase. At temperatures close to 2000 ^{o}C this rate will be rather high and amount to about 2000 atomic layers per second.

During the peritectic reaction, when the liquid and solid phase are interacting, density segregation will occur because of the normally higher density of the α-phase compared with the liquid. In some cases, the density differences are respectable; like for the system Nb-Al with ρ =8.40 g/cm^3 for Al. At elevated temperatures in the liquid state, these differences are somewhat reduced because of the mutual solubility, but they are nevertheless considerable. The effect of density segregation necessitates a much longer diffusion distance for the atoms, and thus results in inhomogeneous and eventually multi-phase samples. Since the transition temperature of A-15 compounds is strongly dependent on stoichiometry and phase status, the superconducting properties of such compounds are normally degraded after a fast cooling through the peritectic temperature region. However, as shown in Table 2, rapid solidification by quenching can also result in higher Tc materials. These effects of stoichiometry, atomic ordering, and impurities on A-15 compounds have been discussed in a separate report [4, 28].

In a containerless environment, the experiments would be designed to nucleate small and homogeneously distributed α-phase particles from an initially single-phase liquid. If the nucleated particles are sufficiently numerous, the peritectic reaction will proceed very rapidly to form the intermetallic phase, since the surface-to-volume ratio of the α-phase particles would also be increased. Thus, containerless low gravity processing can provide improvements over normal processing by introducing homogeneous nucleation, by reducing phase separation and by eliminating crucible contamination.

III. Studies on Droplet Formation

A. Melting Apparatus

A laboratory apparatus suitable for the melting of small alloy droplets was used which was designed and set up in the Space Sciences Laboratory by Dr. Lester Katz of MSFC. A schematic representation of the installation is shown in Fig. 6. The sample in the form of wires or cylindrical rods is melted by electron bombardment from a circular tungsten filament (2 cm diameter). The wire is positioned perpendicular to the filament plane so that the end points right into the filament center, as can be seen in more detail in Fig. 7. The sample can be raised and lowered in respect to the filament in a vertical direction with a gear connection from the outside of the chamber. The filament is on a negative potential of -4 kV, whereas, the sample itself is grounded. The number of bombarding electrons can be regulated by varying the filament current.

The furnace is located in a metal bell jar which can be evacuated to 10^{-6} torr. Observation and photography of the sample or the pendant droplet can be done through two glass windows. The sample can be moved from the outside over a vertical distance of 13 cm by rotation of a knob which connects with the gear box within the vacuum system. The droplet forms on the tip of the wire and its size can be increased by lowering the wire.

Initial test runs with the furnace were performed with copper wires of commercial purity. The wires were available in diameters from 3.0 to

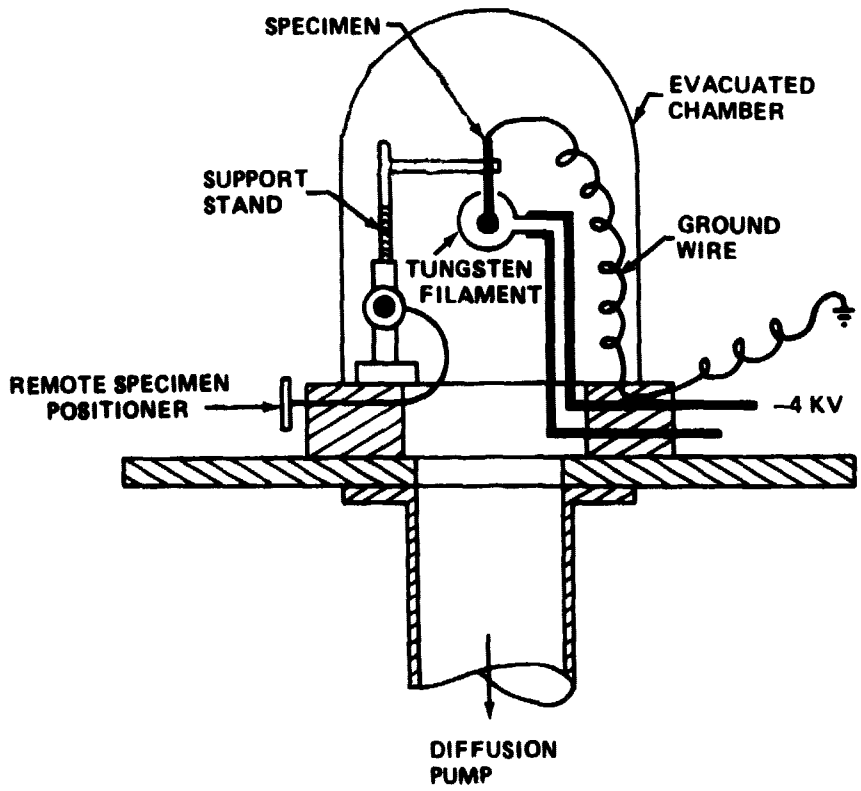

Figure 6. Schematic representation of the electron bombardment furnace for pendant droplet formation.

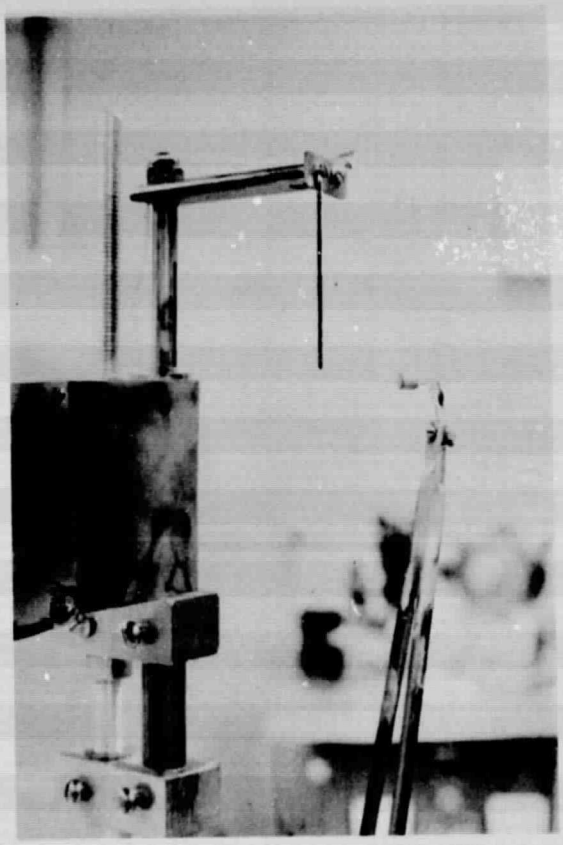

Figure 7. Sample holder with vertically movable direction with copper wire and circular tungsten filament.

0.2 mm. Before the melting, each wire was carefully sanded, straightened and cleaned with acetone. In a typical run, the wire was clamped vertically into the movable bracket. Its end was adjusted such that the wire went straight through the ring-shaped filament. A filament current of about 50 mA, equivalent to a power consumption of 200 W, was normally sufficient to melt the wire. Thereafter, an equilibrium position for the droplet resulted about 1 cm above the filament plane. The filament current could then be left constant and the wire was slowly lowered so that the pendant droplet stayed in a fixed position and grew in size until its fall-off. Sequential photographs of a growing liquid droplet taken through one porthole are given in Fig. 8. A copper wire with a 0.4 mm diameter (Sample No. 13) was used for this demonstration. Since there is no free-fall distance attached to the system, the drop was caught in the liquid state in a ceramic container.

The melting of 10 mil diameter niobium wire proved to be very difficult with the present system. Whereas, the Cu has a melting temperature of 1084 ^{o}C, this melting temperature for Nb is 2470 ^{o}C. In order to improve the efficiency of the bombardment furnace, a circular grid was installed around the filament which was also put on the negative potential of 4 kV. Using this modification, the Nb wire could be melted with a filament current of about 250 mA, equivalent to 1000 W. In the latter stage of this investigation a more powerful high voltage power supply § became available. This instrument can deliver up to 8000 Watt to the source where the filament current and the high voltage can be varied independently. The performance of this power supply has been successfully tested by melting niobium wire and several 3Nb:1Sn powder compacts.

The equipment and instrumentation is designed such that it can be operated by a single person. Remote control of bombardment power is a desirable feature for fast and efficient operation.

B. Droplet Formation

1. Copper

Most of the data on droplet formation have been obtained with copper wire of commercial purity. Various size droplets could be formed

---

§ Airco Temescal, Electron Beam Power Supply, Model CV-8.

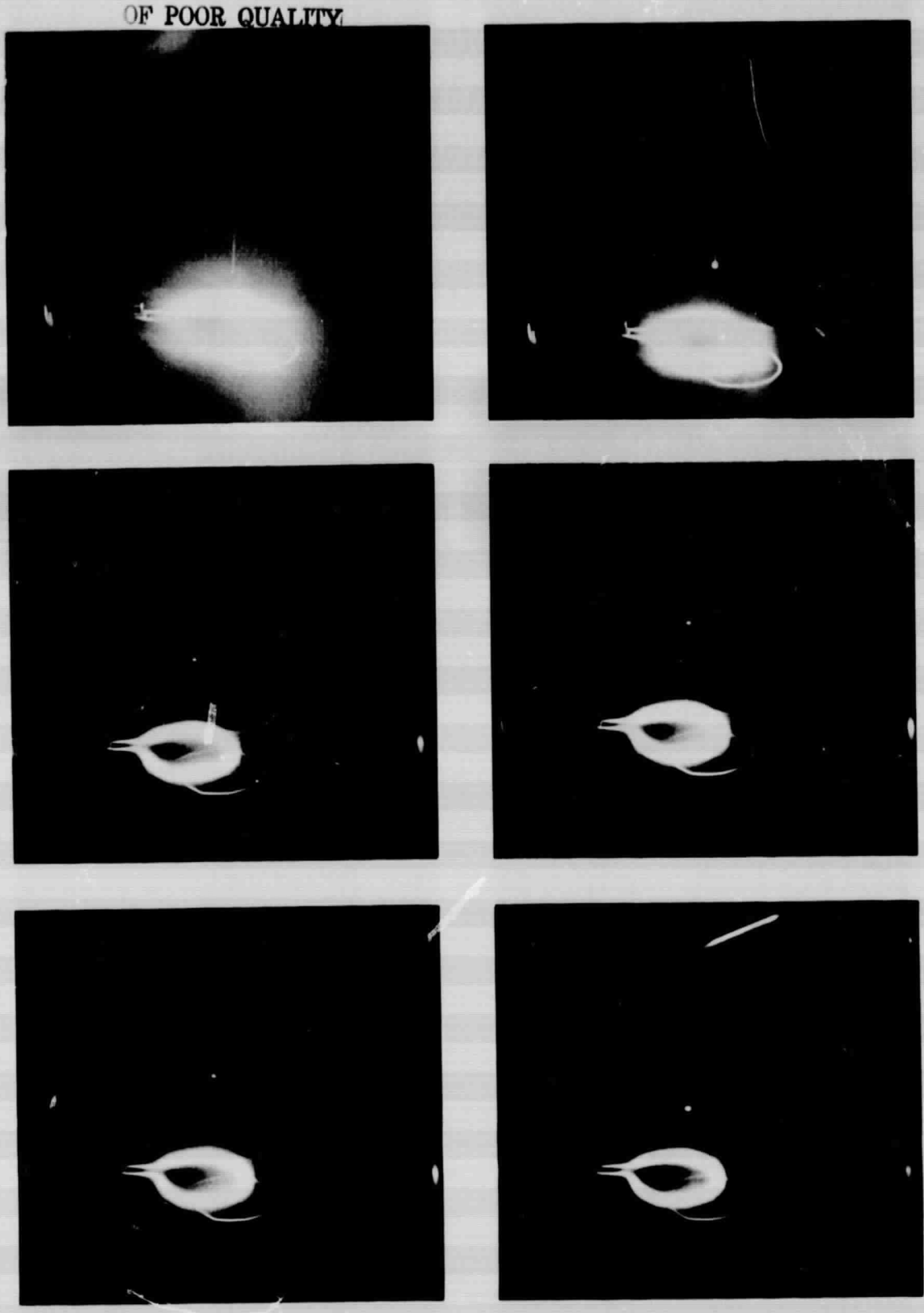

Figure 8. Pendant droplets of copper on a wire with 0.4 mm diameter. The secondary image of the filament is caused by reflection on the thick glass window of the port viewing hole.

by using wires with different diameters. Such a dependency can be expected because the surface tension of a liquid is related to the weight of a drop which separates freely from the end of a wire by the expression [29]

$$\gamma = F(mg/R) \tag{3}$$

where γ is the surface tension, m the critical mass, g the acceleration of gravity, R the radius of the wire and F a function of V/R^3 with V being the volume of the drop. We see from eq. (3) that the mass of the detaching droplet should be proportional to the radius of the wire, since for a given material γ is a constant.

Results of the droplet formation on Cu wires with different diameters are given in Table 3. The mass of the droplet could be determined by either the weight of the material, caught after a free-fall distance of 55 cm, or by a difference measurement of the mass of the wire before and after drop formation. The latter method appears to be more accurate, since no losses due to splashing occurs. In all cases, as can be seen from Table 3, the two masses agree within about 5%. Droplets from wires with a diameter of 0.2 and 0.4 mm could not be made with a single wire and were obtained by stranding together the excess wire over a length of about 5 cm. The strand was constructed such that the drop released in the single-wire region after the stranded portion had been melted.

In Fig. 9, the critical masses (M_1) of the droplets are plotted against the diameters of the copper wires. We notice a nearly linear relationship between the data points. However, the quality of the fit will improve once the correction factor F has been applied to the raw data, as will be done later.

Small oscillations of the drop before separation could not be avoided. These instabilities were observed to be less pronounced for larger diameter wires. The tendency to oscillate increased with melting temperature of the element, since more bombardment power was required for drop formation. Strong oscillations may lead to a premature detachment of the drop. Some liquid metal was left on the stem after the drop had fallen off. These corrections are significant for the large

TABLE 3

SUMMARY OF DATA FOR DETACHED COPPER DROPLETS

Sample Number	Wire Diameter D(mm)	Mass of Droplet from wire M_1 (mg)	Mass of Droplet by Weight M_2 (mg)	Deviation $\frac{M_1-M_2}{M_2} \times 100(\%)$	Length of of Wire Needed (mm)	Diameter * of Sphere d(mm)
12	3.0	709	-	-	11.2	5.33
9	2.58	625	620.5	0.7	13.3	5.11
10	2.58	621	618	0.5	13.2	5.10
6	2.0	476	1,388	2.9	16.9	4.66
7	2.0	490		5.9	17.4	4.71
8	2.0	482		4.2	17.1	4.68
15	1.3	321.7	320	0.5	27.0	4.09
16	1.3	337.6	342.6	-1.5	28.4	4.16
1	0.79	175	168	4.2	39.8	3.34
2	0.79	179	167	7.2	40.8	3.37
3	0.79	181	175	3.4	41.2	3.38
4[+]	0.79	-	195.5	-		-
5	0.79	172	165	4.2	39.2	3.32
11	0.4	111.8	113.1	-1.2	99.3	2.88
14	0.4	121	-	-	107	2.95
13[+]	0.4	123.5	-	-		-
17	0.4	117.2	121.4	-3.5	104	2.92
18	0.2	58.6	56.3	4.1	208	2.32

* Calculated from M_1 with $\rho(Cu) = 8.96\ g/cm^3$ at room temperature

[+] For photography. Droplet solidified on wire.

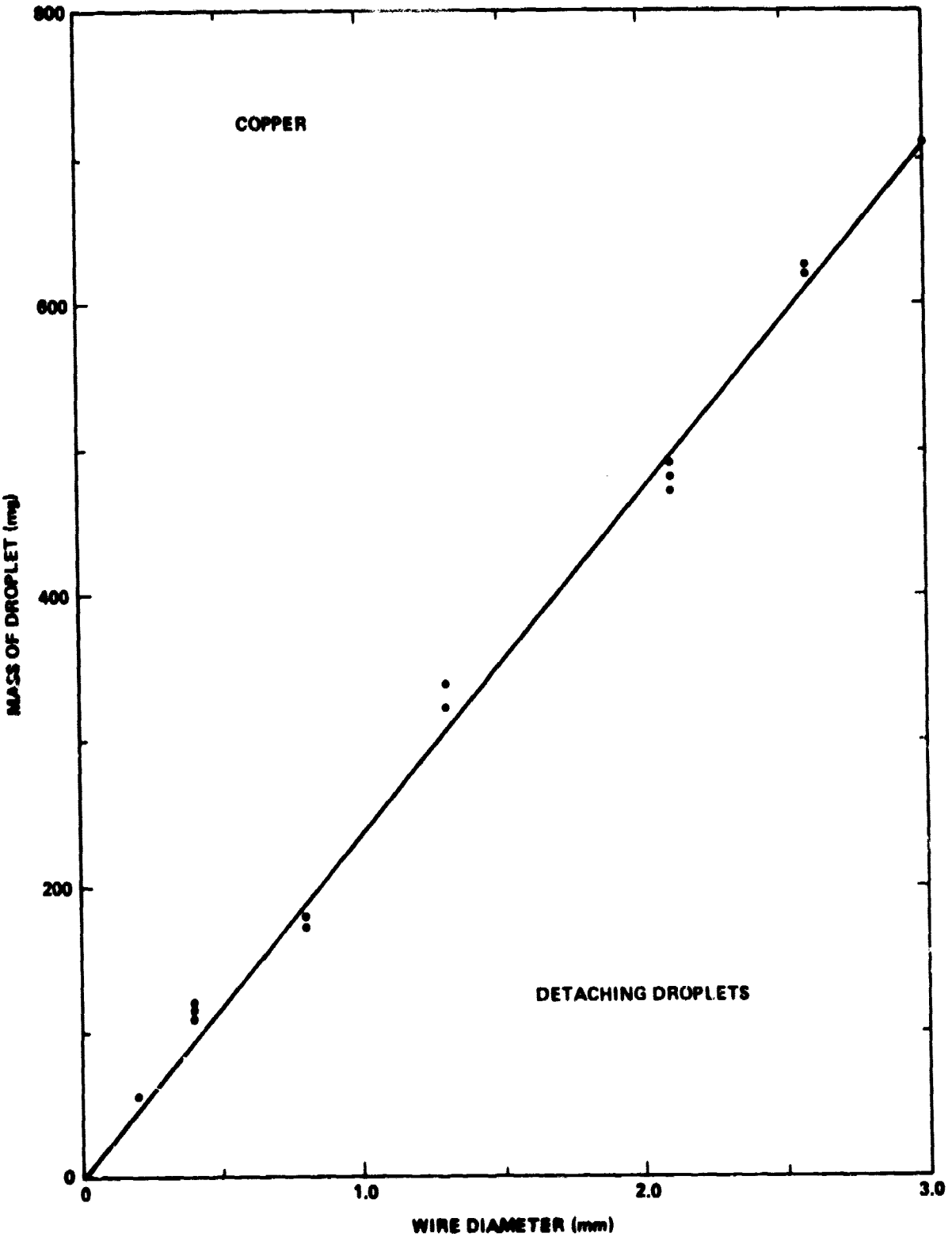

Figure 9. The critical masses of droplets falling from copper wires with different diameters.

diameter wires, whereas, they are less important for the thin wires. The detachment of the droplets occurs without any prior indication. The formation of a secondary satellite droplet has not been observed.

2. Niobium

The results on droplet formation with niobium wire of 5 and 10 mil diameter wire are given in Table 4 and Fig. 10. These droplets were also obtained by melting a 5 cm long stranded portion of wire over a total length of 13 cm. The droplets fell off from the single strand of wire after the stranded length had been melted. After a free-fall distance of 55 cm in the bell jar, the drop was caught in a ceramic container. In contrast to the experiments with copper, the niobium droplet did not splatter apart in several smaller droplets, and solidified as a single, but flattened piece of material. It may be noted that due to the high surface tension of niobium, the diameter of the droplet which can be suspended is more than ten times the diameter of the wire. These conditions are reflected in the insert of Fig. 10 which depicts a photograph of an about critical niobium sphere suspended from 10 mil diameter wire.

A summary of the critical masses of copper in relation to niobium droplets is given in Fig. 11. The unity slope in this logarithmic graph represents the linear relationship between the droplet mass and the wire diameter. The different surface-tension values for liquid Cu and Nb are expressed by the offset of the curves.

3. Niobium-Tin Alloys

For the preparation of Nb_3Sn a powder compact, consisting of a mixture of 75 at. % niobium and 25 at. % tin, was used. This mixture which was contained in a cylindrical copper tube had been compacted by shock waves [30]. It has been already shown [31] that it is possible under high pressure conditions to form the compound Nb_3Sn from its constituents. However, the starting powders used here were compacted with a sub-critical load so that the intermetallic compound did not form. These conditions were confirmed by superconductivity measurements.

The shock wave compacted sample was cut with a diamond saw into rectangular columns with a width of about 1.5 mm and a length of 40 mm. Initially, 10 mil diameter niobium wire was attached to the upper part of the compact as shown in the shadowgraph of Fig. 12a. The mechanical

TABLE 4

SUMMARY OF DATA FOR DETACHED NIOBIUM AND VANADIUM DROPLETS

Sample Number	Wire Diameter D(mm)	Mass of Droplet from Wire M_1 (mg)	Mass of Droplet by Weight M_2 (mg)	Deviation $\frac{M_1-M_2}{M_2} \times 100(\%)$	Length of of Wire Needed (mm)	Diameter* of Sphere d(mm)
Niobium						
20	0.254	131.2	131.0	0.2	308	3.10
21	0.254	136.3	135.8	0.4	320	3.14
22	0.127	68.6	68.2	0.6	645	2.50
19†	0.254		101	-	-	2.84 2.82a
23	0.254	128.8	128.5	0.2	303	3.08
Vanadium						
24	0.127	69.5	69.1	0.6	900	2.79

* Calculated from M_1 with $\rho(Nb) = 8.4\ g/cm^3$, $\rho(V) = 6.1\ g/cm^3$ at room temperature

† Droplet solidified on wire

a Measured value

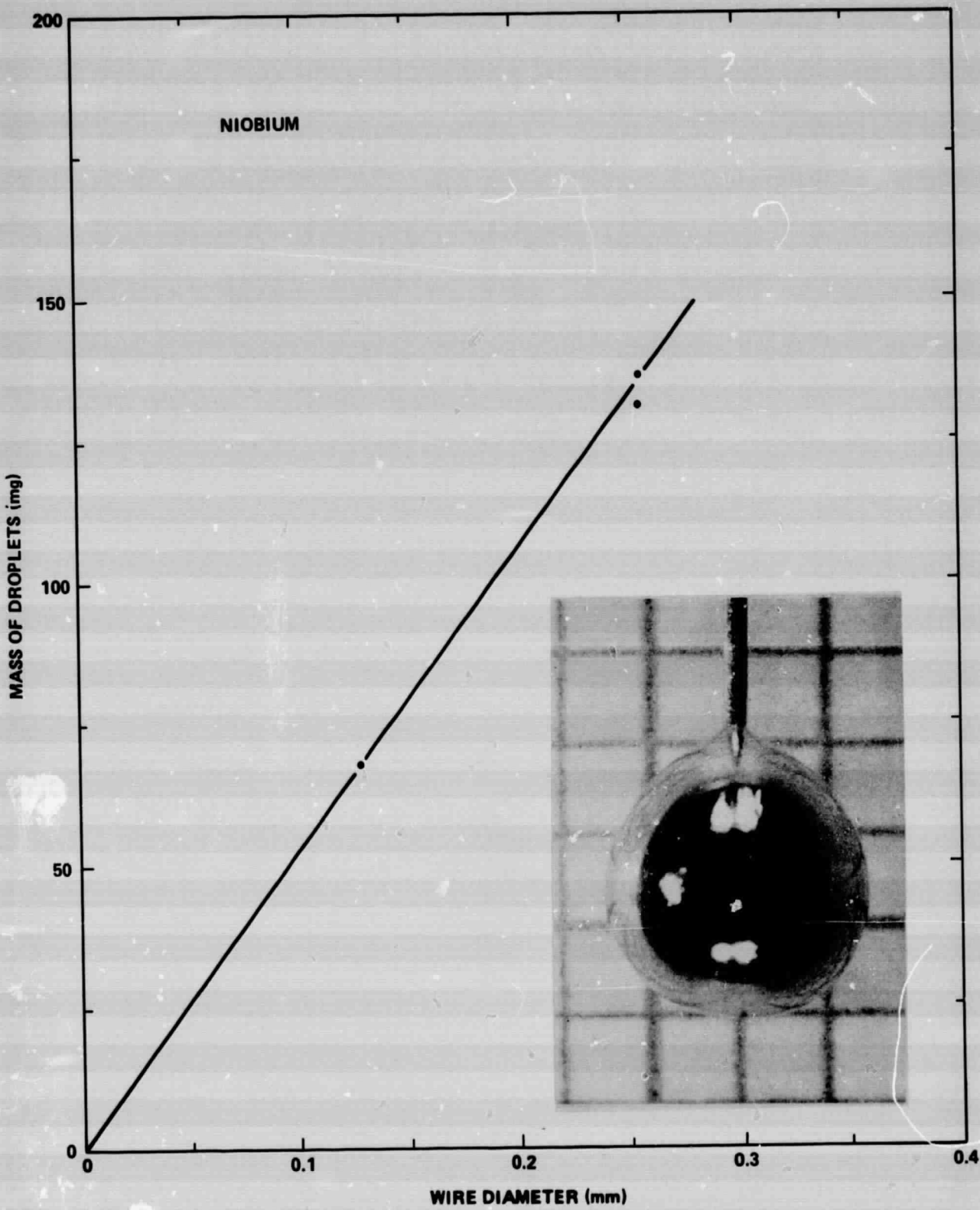

Figure 10. The critical masses of droplets falling from niobium wires with different diameters. Insert: Solidified niobium sphere of about critical mass suspended from 10 mil diameter wire. Each division of the background grid represents 1 mm.

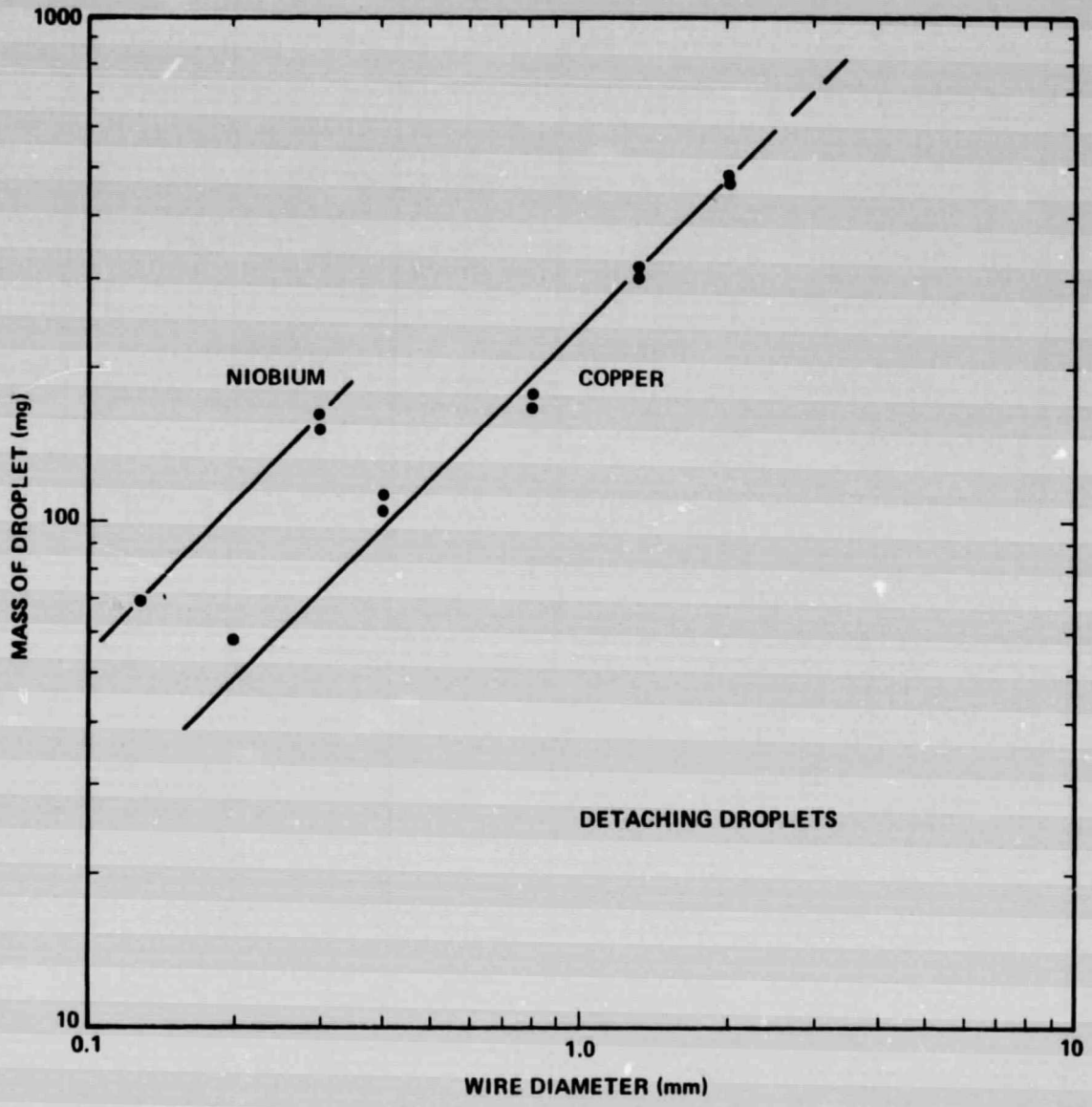

Figure 11. The critical masses of copper and niobium droplets from different diameter wires. Summary of data on a logarithmic scale.

contact obtained by wrapping the Nb wire one time around the sample gave a good electrical connection. However, it was found that such an arrangement was very susceptible to oscillations and so the 10 mil Nb wire was replaced by a 20 mil tungsten wire. A shadowgraph of a so prepared sample is given also in Fig. 12b. The tungsten wire gave good stability and did not melt even under high emission currents. Contamination of the compact by tungsten was possible only in the upper portion of the sample which could not be used anyway.

A droplet of critical size falling off the compact could be obtained by slowly increasing the filament current and leaving the accelerating voltage constant (5 kV).

C. Determination of Surface Tension

The phenomenon of surface tension and surface energy of liquids are the result of incomplete atomic coordination at the surface. A force perpendicular to the boundary is exerted, thus minimizing the surface area. Liquid surface-tension data refer to the interface between the liquid and its own vapor or a nonreactive atmosphere.

The critical masses of the detached droplets can be used to calculate surface-tension values according to Eq. (3). However, corrections have to be applied to this relation since not all the liquid metal which contributes to the detachment of the droplet actually falls off the wire. In practice, a weight m'g is obtained which is less than the ideal value mg, which leads to the correct value for the surface-tension and is given by

$$\gamma = mg/2\pi Rf \qquad (4)$$

A schematic sequence of a detaching drop, taken from high-speed photographs by Adamson [29] is given in Fig. 13. For large rod diameters, a large amount of remaining liquid is observed and eventually a thin cylindrical neck develops which may lead to a secondary droplet. The dimensionless correction factor f has been determined for common liquids by several authors and is normally given as a function of the wire radius, R, divided by the cube root of the experimentally-measured volume, $V^{1/3}$.

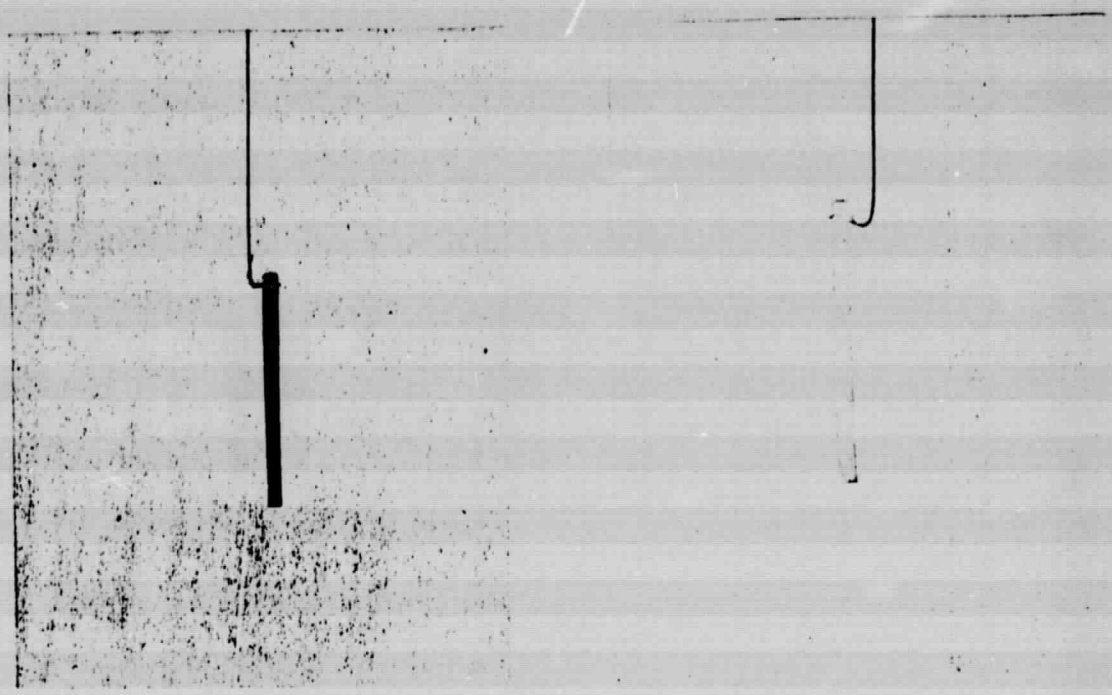

12a 12b

Figure 12: Shadowgraphs of compacted 3Nb:1Sn powder samples. a) Sample on 10 mil Nb wire b) Sample on 20 mil W wire.

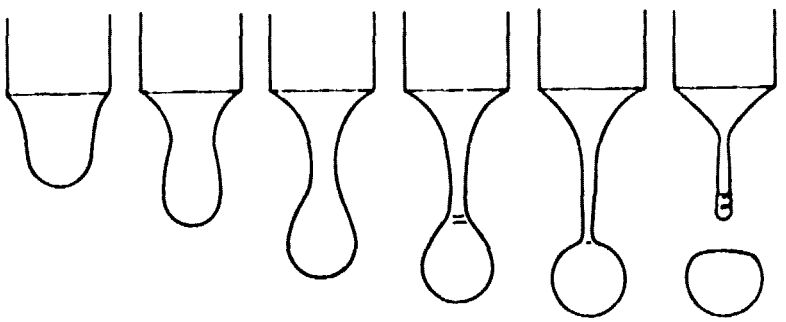

Figure 13. Schematic Sequence of a separating drop derived from high speed photographs [29].

The correction factors for various size droplets from ref. [29] are given in Table 5. It may be noted that the factor f is fairly constant for $R/V^{1/3}$ values in the region of 0.6 to 1.2. For our data $R/V^{1/3}$ varies between zero and 0.35 and f correspondingly between 1 and 0.7. The table is used as follows: From the experimental value of m, the droplet volume is determined via the density of the liquid metal and, $R/V^{1/3}$ is calculated.

TABLE 5

Correction Factors for the Drop Weight Method

$R/V^{1/3}$	f	$R/V^{1/3}$	f
0.00	(1.0000)	0.75	0.6032
0.05	0.945*	0.80	0.6000
0.10	0.89*	0.85	0.5992
0.15	0.84*	0.90	0.5998
0.20	0.80*	0.95	0.6034
0.25	0.76*	1.00	0.6098
0.30	0.7526	1.05	0.6179
0.35	0.7011	1.10	0.6280
0.40	0.6828	1.15	0.6407
0.45	0.6669	1.20	0.6535
0.50	0.6515		
0.55	0.6362		
0.60	0.6250		
0.65	0.6171		
0.70	0.6093		

* Graphically interpolated values from [29]

Surface-tension data derived from eq. (4) for copper, niobium and vanadium are given in Tables 6 and 7. For the various diameter Cu wires, the correction factor changes between 0.7 and 1.0. The average surface-tension value obtained for copper can be given as 1015 $\pm$ 50 dyne/cm.

TABLE 6: CORRECTION VALUES AND DERIVED SURFACE-TENSION DATA FOR COPPER

Surface Number	Wire Diameter D(mm)	Mass of Droplet M_1 (mg)	$R/V^{1/3}$	Surface Tension* (dyne/cm)
12	3.0	709	0.335	1053
9	2.58	625	0.301	1057
10	2.58	621	0.302	1052
6	2.0	476	0.256	998
7	2.0	4.90	0.253	1027
8	2.0	482	0.254	1010
15	1.3	321.7	0.189	964
16	1.3	337.6	0.186	1015
1	0.79	175	0.141	825
2	0.79	179	0.140	844
3	0.79	181	0.139	851
4	0.79	drop solidified on wire		
5	0.79	172	0.142	810
11	0.4	111.8	0.083	968
14	0.4	121	0.081	1048
13	0.4	123.5	0.080	-
17	0.4	117.2	0.082	1017
18	0.2	58.6	0.051	970

TABLE 7: CORRECTION VALUES AND DERIVED SURFACE-TENSION DATA FOR NIOBIUM AND VANADIUM

Sample Number	Wire Diameter D(mm)	Mass of Droplet M_1 (mg)	$R/V^{1/3}$	Surface Tension* (dyne/cm)
Niobium				
20	0.254	131.2	0.099	1812
21	0.254	136.3	0.098	1882
22	0.127	68.6	0.062	1785
19	0.254	drop solidified on wire		
23	0.254	128.8	0.099	1779
Vanadium				
24	0.127	69.5	0.055	1808

*Calculated liquid density for niobium 7.8 g/cm^3 and for vanadium 5.55 g/cm^3

In this average, the values for samples No. 1 to 5 with a wire diameter of 0.79 mm have not been included because these data seem to be erroneous and it is possible that the chemical composition of this wire was different from the others. The surface-tension values obtained from the different diameter wires are plotted in Fig. 14. Literature values [32] for pure Cu range from 1220 to 1350 dyne/cm. The fact that our surface-tension data are always somewhat lower than those reported in the literature may be caused by dissolved impurities in the copper wires of commercial purity. The average surface-tension data obtained for niobium (1815 $\pm$ 60 dyne/cm) and vanadium (1810 dyne/cm) show a better agreement with the data reported in the literature. These are 1900 and 1920 dyne/cm for Nb and V, respectively [32].

D. Evaporation Losses

1. Experimental Data for Cu and Nb

Evaporation from suspended metal droplets can be expected due to considerable vapor pressure at the melting temperature. In the following, we will describe the experiments conducted for pure copper and niobium, which will lead to an estimate of evaporation losses from multicomponent alloys.

Evaporation losses as a function of time from a free surface of liquid copper were determined. Forming a droplet of sub-critical size by melting 2.0 cm of 0.7 mm diameter wire, the experiment was run for 15 minutes and then interrupted for a mass measurement of the whole wire and a determination of the droplet diameter. Afterwards the experiment was continued for another 15 minutes. No difficulties in remelting the sphere were experienced. However, melting of some additional Cu-wire occurred before a new equilibrium position for the droplet could be achieved. Sustaining the equilibrium position of the drop was a very delicate task and any small perturbation in filament current or acceleration voltage resulted in an upward movement of the pendant droplet. A clear distinction of the liquid or solid state of the droplet was possible by observing its surface. A reflection of the glowing filament wire in the liquid state was clearly visible but no image could

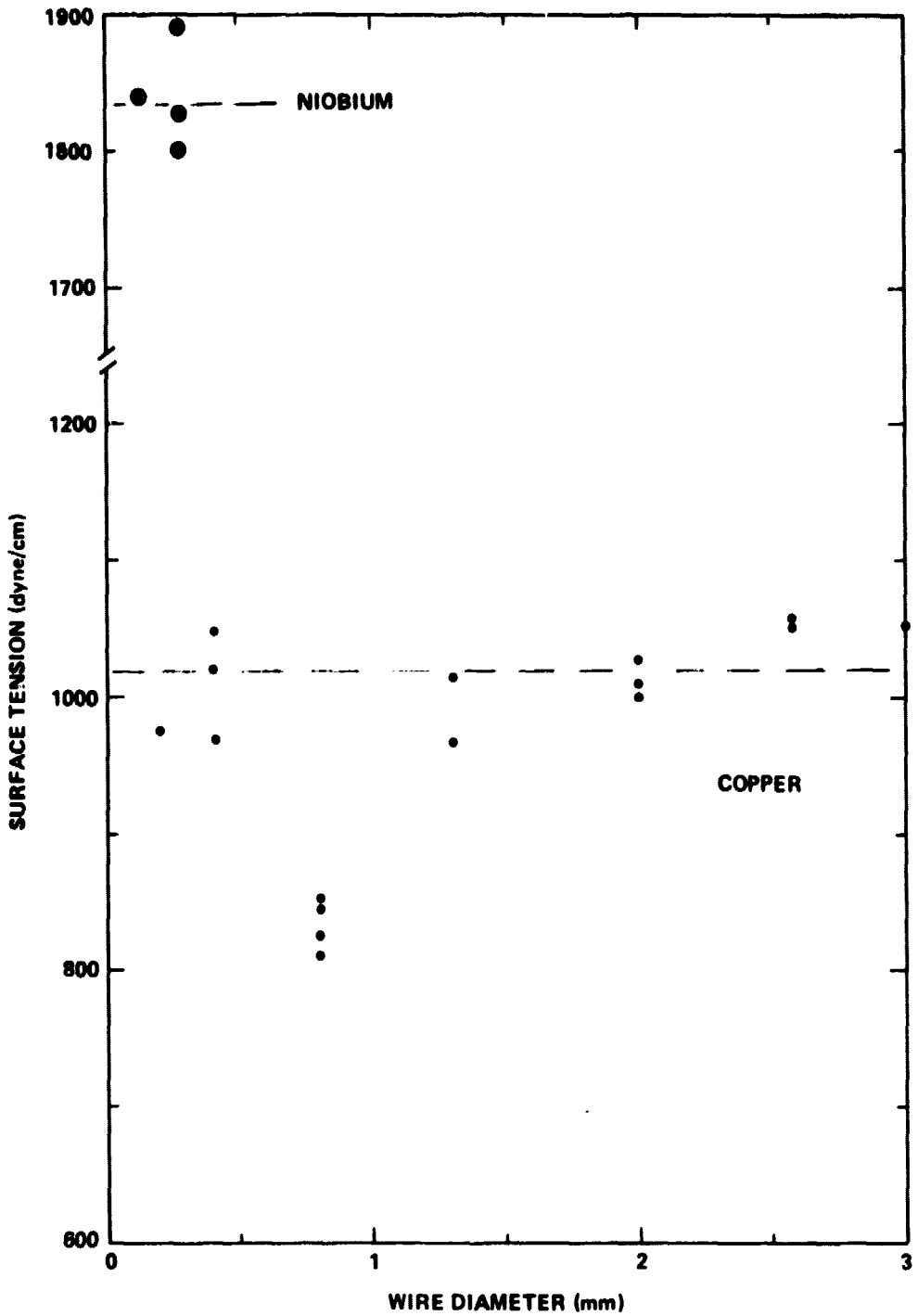

Figure 14. The surface tension of copper and niobium as derived from wires with different diameters.

be observed when the drop was solid. The progression of the solid/liquid interface for a slowly solidifying drop was very distinct.

This particular evaporation experiment was run five times for a duration of 15 minutes each before the droplet mass became critical and separation occurred. The results obtained are summarized in Table 8. It can be seen that evaporation rates in the order of 10^{-4} g/min are observed in this case. In other words, approximately 0.1% of the droplet weight per minute is lost by evaporation at the melting temperature. After consideration of the changing surface area for the suspended droplet an average evaporation rate can be given as $3.8 \pm 0.7 \times 10^{-6}$ g $mm^{-2}min^{-1}$. Because of the qualitative nature of the experiment, no correction for thermal expansion of the metal was made. It was also assumed that evaporation occurs only from the total surface of the pendant droplet.

In respect to the strong dependency of the surface-tension on impurities like oxygen and nitrogen, it is of interest to express the evaporation rate by the number of atomic layers leaving the surface in unit time. For copper, we find that this rate is equivalent to about 30 atomic layers per second. According to the kinetic theory of gases, about two atomic layers of air per second impinge on the drop surface at 5×10^{-6} torr [33]. Since the evaporation rate of copper from the surface at this working pressure is appreciably higher than the rate of impinging impurity atoms, the surface of the liquid droplet is well protected from residual gas contamination below a pressure of 10^{-4} torr.

Evaporation measurements have also been performed with niobium wire of 10 mil diameter. A pendant droplet of about 1.5 mm radius was suspended for a duration of five minutes. Thereafter, the top of the bell jar heated noticeably. A weight loss of 21.9 mg was determined for this period. The niobium droplet could be remelted afterwards but an equilibrium position could not be reached fast enough, before detachment occurred. The data obtained for this single experiment with niobium are also given in Table 8. We may note that the evaporation rates for liquid Nb are about ten times as much as those for copper. However, the melting temperature of the two elements is also considerably different. About 400

TABLE 8

Measured Evaporation Rates for Copper and Niobium

Copper (T=1083 ^{o}C)

Droplet Radius (mm)	Surface Area[&] (mm^2)	Weight Loss (mg/15 min)	Evaporation Rate ($\mu g\ mm^{-2}\ min^{-1}$)
1.395	24.4	1.1	3.0
1.54	29.8	1.6	3.6
1.575	31.2	1.8	3.85
1.63	33.4	2.4	4.8
1.63	33.4	1.9	3.8

Niobium (T=2500 ^{o}C)

1.5	28.3	21.9[§]	52

§ Result obtained from experiment of 5 minutes duration.

& No correction for thermal expansion applied.

atomic layers per second leave the niobium surface and, therefore, the Nb droplet is even better protected from impinging residual gas atoms than is the copper surface.

2. Calculation of Evaporation Rates

The experimental evaporation losses reported here were for Cu and Nb at their melting points. In regard to the future melting of multi-component alloys where at least one component is heated high above the melting temperature of the other, it would be desirable to calculate evaporation rates from first principles.

Below pressures of 10^{-1} torr, the vapor molecules can be assumed to leave the emitting surface relatively unimpeded. Under these circumstances Langmuir [34] derived the following equation for the rate of evaporation in vacuum per unit area and unit time:

$$R = 5.85 \times 10^{-2}\ a\ P\sqrt{\frac{M}{T}}\ \ (g\ cm^{-2}sec^{-1}) \qquad (5)$$

where P is the vapor pressure in mm Hg at the absolute temperature T, M is the atomic weight of the material being evaporated, and a is the sticking probability of atoms condensing at the surface areas. For our purpose, we will reasonably assume a = 1, which means that all the vapor atoms arriving at the wall of the bell jar will also condense there.

Evaporation rates for some elements of interest at their respective melting temperatures have been calculated with eq. (5) and are listed in Table 9 along with vapor pressure data at the melting point. We can see from these data that the evaporation rates for different materials can vary over several, orders of magnitude. A relatively low evaporation rate of 10^{-8} g $cm^{-2}sec^{-1}$ is indicated for vanadium at the melting point. In the last column of table 9, the experimental rates for Cu, Nb and Cr are also listed. Considering the limited accuracy of the experiment, the agreement of the two evaporation rates is very good and justifies the application of eq. (5) to temperatures above the melting point for liquid alloys.

TABLE 9

Calculated and Measured Evaporation Rates for Selected Elements

Element	Melting Temp. (K)	Vapor Pressure (mm Hg)	Calc. Evap. Rate ($g\ cm^{-2}sec^{-1}$)	Meas. Evap. Rate ($g\ cm^{-2}sec^{-1}$)
Copper	1356	3.5×10^{-4}	4.4×10^{-6}	6.3×10^{-6}
Chromium	2173	8	7.2×10^{-2}	6.2×10^{-2} [34]
Vanadium	1970	1×10^{-6}	9.4×10^{-9}	-----
Niobium	2773	5×10^{-3}	5.4×10^{-5}	8.7×10^{-5}
Tantalum	3270	6×10^{-3}	8.3×10^{-5}	-----
Tungsten	3650	2×10^{-2}	2.6×10^{-4}	-----

3. Evaporation Rates for A-15 Compounds

Evaporation rates for the elements Ga, Sn, Al, Ge, Cu, Au, Si, Pt, and V at temperatures above their respective melting temperature were calculated with eq. (5) and the results are plotted in Fig. 15. The vapor pressure data from various handbooks [5, 6] have been used for this graph. Those elements listed above are constituents for high transition temperature superconductors with the A-15 structure. Normally, in these compounds, a non-transition element, like Ga, Al, Sn, or Si is combined with a transition element, like niobium or vanadium. To form a compound like Nb_3Sn, three parts of Nb have to react with one part of Sn. Most of the A-15 compounds form by a peritectic reaction at about 1800 ^{o}C. We can see from Fig. 15 that at this reaction temperature, which is always below the melting temperature of the particular transition element involved, the evaporation rates for Nb or V are very small and in the order of 10^{-6} g $cm^{-2}sec^{-1}$. However, as can be seen from the figure, the vapor pressure of the second components are larger by several orders of magnitude.

We can conclude from Fig. 15 that evaporation losses will be high when preparing the compounds V_3Ga or Nb_3Ga. The least losses should be expected with V_3Si or Nb_3Si. The calculated losses for tin and aluminum compounds are located inbetween. It is remarkable that the com-

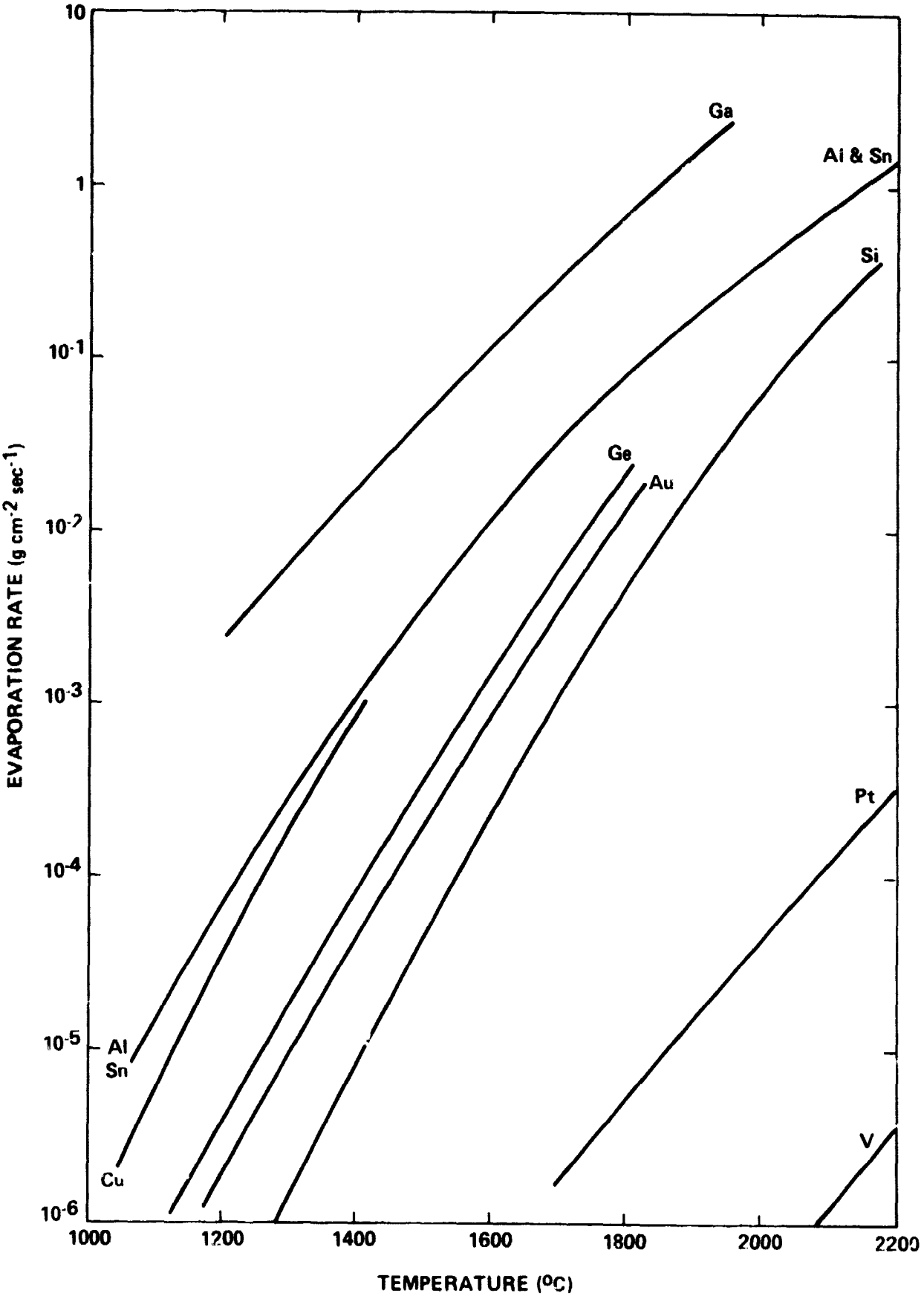

Figure 15: Evaporation rates for various elements as a function of temperature.

pound Nb_3Pt or V_3Pt should form with a very small evaporation rate of the second component (Pt) which is several orders of magnitude below the rates of all the compounds mentioned before.

Using the data from Fig. 15, an evaporation rate of 7×10^{-5} g cm^{-2} sec^{-1} is expected when preheating Nb-Sn powders at about 1200 ^{o}C. Experimentally, during a particular preheating experiment of a Nb-Sn powder compact for 15 minutes, a loss of 200 mg was registered which corresponds - using the known sample dimensions - to a rate of approximately 9×10^{-5} g cm^{-2} sec^{-1} for Sn. This agreement again justifies application of eq. (5) for estimating low temperature evaporation rates. When calculating the evaporation rate for a compound the atom fraction of the second component must be considered.

In order to minimize evaporation of the second component several precautions can be taken. The heating of the samples and the drop formation should be done in the shortest time possible. For metallic wires this procedure can be accomplished during several seconds. Preparing A-15 compounds by the conventional technique of arc-melting evaporation losses of approximately 1% are experienced during a melting time of about 20 seconds. When the losses are known they can be compensated for by putting an excess of the second component into the starting material. In addition, these powder compacts can be pre-heated at about 1000 ^{o}C so that diffusion of the volatile component into niobium or vanadium can occur. Another possibility to minimize evaporation losses would be to start with an arc-melting of which already contains the compound phase.

IV. Conclusions and Recommendations

The technique of electron bombardment proved to be a suitable method for generating liquid droplets of metallic materials. No spurious accelerations were imparted on a detaching drop with the circular shape of the filament used.

The surface tension of liquid metals sensitively depends on the cleanliness of the surface. However, it was shown that for copper and niobium at working pressures of 10^{-5} torr no contamination of the surface by residual gases will occur. The size of the detaching drop can be controlled by the diameter of the supporting wire. The ability to vary the droplet diameter is necessary since the free-fall distance in the tube must be matched with the time required for solidification.

Cooling rate and solidification time depend on the total emissivity of the metal which, in most cases, is not known very accurately. Therefore, an independent means for establishing the total solidification time of the drop is desirable. This task may be achieved by photographing the drop during free-fall at various locations.

Evaporation losses may be encountered when melting alloys with multiple components. A depletion will take place mainly in the surface layers since the transport of the evaporating phase is limited by liquid state diffusion. These losses can be compensated for by a surplus of the low melting component, once a routine procedure for the drop formation is established. In addition, the utilization of pre-diffused material or an already reacted compound is recommended for keeping evaporation losses low.

A drop tube will allow practising the principle of containerless and low gravity processing. Although the time span of several seconds will not be sufficient to obtain optimum samples the trends of selected parameters can be used to determine the improvements resulting from low gravity processing and can lead to a longer term experiment as for example on a sounding rocket or Spacelab flight.

V. References

1. "Proceedings of the Third Space Processing Symposium - Skylab Results," NASA M-74-5, June 1974.

2. "Apollo-Soyuz Test Project: Preliminary Science Report," NASA TMX-58173, Feb. 1976.

3a. L. Katz: "Drop Tube Design and Operation for Simulating Low Gravity Load Space Processing Experiments," Memorandum, Marshall Space Flight Center, June 1976.

3b. J. Reger: "Experimental Development of Processes to Produce Homogenized Alloys of Immiscible Metals." Final Report for NASA Contract NAS8-27805. January 1973.

3c. A. Lorenz: "Plant Facility for Zero Gravity Experiments." DFVLR - Nachrichten, Issue 14, p. 563 (1974).

4. G. H. Otto and L. L. Lacy: "Current Materials Research Associated with High Transition Temperature Superconductors," Memorandum, Marshall Space Flight Center, August 1975.

5. CRC Handbook of Tables for Applied Engineering Science, The Chemical Rubber Co., Cleveland, Ohio, 1970.

6. CRC Handbook of Chemistry and Physics, 55th Edition, The Chemical Rubber Co., Cleveland, Ohio, 1975.

7. G. R. Johnson and D. H. Douglass: "A-15 Phases: Occurrence, Geller Radii, and Electronic Structure." J. of Low Temp. Phys. 14, 565 (1974).

8. M. Weger: Rev. Mod. Phys. 36, 175 (1965). J. Phys. Chem. Solids 31, 1671 (1970).

9. "Columbium adn Tantalum" F.T. Sisco Ed., John Wiley, New York, N.Y., 1963, p. 457.

10. C. E. Lundin and A. S. Yamamoto: Trans. Metall. Soc. AIME 236, 863 (1966).

11. J. H. N. van Vucht, D. J. van Ooijen and H. A. C. M. Bruning: Philips Res. Repts. 20, 136 (1965).

12. H. A. C. M. Bruning: Philips Res. Repts. 22, 349 (1967)

13. J. H. N. van Vucht, H. A. C. M. Bruning, H. C. Donkersloot and A. H. Gomes de Mesquita, Philips Res. Rpts. 19, 407 (1964).

14. G. W. Webb in "Superconductivity in d- and f- Band Metals", D. H. Douglass, Ed. American Institute of Physics, New York, N.Y., 1972, p. 139.

15. J. R. Gavaler, M. A. Janocko, A. I. Braginski, and G. W. Roland: IEEE Transactions on Magnetics, MAG-11, 192 (1975).

16. B. T. Matthias, T. H. Geballe, R. H. Willens, E. Corenzwit, and G. W. Hull: Phys. Rev. 139, A1501 (1965).

17. G. Otto: Z. für Physik 215, 323 (1968).

18. S. Foner, E. J. McNiff, Jr., B. T. Matthias, T. H. Geballe, R. H. Willens, and E. Corenzwit: Phys. Lett. 31A, 349 (1970).

19. S. Foner, E. J. McNiff, Jr., T. H. Geballe, R. H. Willens, and E. Buehler: Superconductivity, F. Chilton ed., North Holland, Amsterdam 1971, p. 534.

20. K. Hechler, G. Horn, G. Otto, and E. Saur: J. Low Temp. Physics 1, 29 (1969).

21. G. Otto: Z. für Physik 218, 52 (1969).

22. S. Foner, E. J. McNiff, Jr., G. W. Webb, L. J. Vieland, R. E. Miller, and A. Wicklund: Phys. Lett. 38A, 323 (1972).

23. R. Flukiger, P. Spitzli, F. Heiniger, and J. Muller: Phys. Lett. 29A, 407 (1969).

24. E. Roschel, O. Loebich and C. J. Raub: Z. Metallkunde 64, xxx (1973).

25. M. Hansen: Constitution of Binary Alloys, First Supplement, McGraw-Hill Book Co., New York, 1965.

26. R. P. Elliott: Constitution of Binary Alloys, First Supplement, McGraw-Hill Book Co., New York, 1965.

27. F. A. Shunk: Constitution of Binary Alloys, Second Supplement, McGraw-Hill Book Co., New York, 1969.

28. Ref. 4

29. A. W. Adamson: "Physical Chemistry of Surfaces," Interscience Publishers, New York, N.Y., 1967.

30. G. H. Otto: "The Effects of Shock Wave Compaction of the Transition Temperatures of A-15 Structure Superconductors." NASA-CR-120708, Final Report for Contract NAS8-30244, August 1974.

31. G. H. Otto, U. Roy and O. Y. Reece: J of Less-Common Metals 32, 355 (1973).

32. "Liquid Metals," S. Z. Beer, Ed., Marcel Dekker, Inc., New York, 1972, p. 186.

33. For example, see S. Dushman: "Scientific Foundations of Vacuum Techniques." John Wiley and Sons, New York, 1949.

34. See L. Holland: "Vacuum Deposition of Thin Films," Chapman and Hall, London, 1966, p. 104.